Cell Biochemistry and Biophysics
https://doi.org/10.1007/s12013-024-01249-1

ORIGINAL PAPER

Effects of Hypoxia and Reoxygenation on Metabolic Profiles of Cardiomyocytes

Luis Daniel Montañez Condori[1] · Cristofher Victor Vivas[1] · Yan Borges Barreto[1] · Ligia Ferreira Gomes[1] · Adriano Mesquita Alencar[1] · Antonio Carlos Bloise[1]

Accepted: 5 March 2024

Abstract

In vitro cellular models provide valuable insights into the adaptive biochemical mechanisms triggered by cells to cope with the stress situation induced by hypoxia and reoxygenation cycles. The first biological data generated in studies based on this micrometric life-scale has the potential to provide us a global overview about the main biochemical phenomena presented in some reported preconditioning therapies in life-scale of higher dimensions. Thus, in this study, a cell incubator was designed and manufactured to produce a cellular model of heart hypoxia followed by reoxygenation (HfR) through consecutive repetitions of hypoxia-normoxia gas exchange. Samples of cellular extracts and culture media were obtained from non-proliferative cardiomyocytes (CMs) cultivated under challenging HfR (stressed CMs) and regular cultivation (unstressed CMs) in rounds of four days for each case. Metabolomic based on proton magnetic resonance spectroscopy (^{1}H-MRS) was used as an analytical approach to identify and quantify the metabolomes of these samples, the endo- and exo-metabolome. Despite the stressed CMs presented over 90% higher cellular death rate compared to the unstressed CMs, the metabolic profiles indicates that the surviving cells up-regulate their amino acid metabolism either by active protein degradation or by the consumption of culture media components to increase coenzyme A-dependent metabolic pathways. This cell auto-regulation mechanism could be well characterized in the first two days when the difference smears off under once the metabolomes become similar. The metabolic adaptations of stressed CMs identified the relevance of the cyclic oxidation/reduction reactions of nicotinamide adenine dinucleotide phosphate molecules, $NADP^+$/NADPH, and the increased tricarboxylic acid cycle activity in an environment overloaded with such a powerful antioxidant agent to survive an extreme HfR challenge. Thus, the combination of cellular models based on CMs, investigative methods, such as metabolomic and ^{1}H-MRS, and the instrumental development of hypoxia incubator shown in this work were able to provide the first biochemical evidences behind therapies of gaseous exchanges paving the way to future assays.

Keywords Hypoxia followed by reoxygenation · Hypoxia · Normoxia · Cardiomyocytes · Proton magnetic resonance spectroscopy · Metabolomics

Introduction

According to the World Health Organization (WHO), cardiovascular diseases are the leading cause of premature death and disability in humans, and their incidence is increasing globally [1]. Typically, cardiovascular diseases represent a cluster of disorders associated with the heart, vasculature of the brain, or blood vessels and predominantly include coronary and ischemic heart disease, deep vein or arterial thrombosis, and cerebrovascular disease [2]. In addition, a range of other modifiable risk factors, such as poor diet, chemotherapeutic drugs, and hypoxia, also contribute to the progression of cardiovascular diseases [3–5].

As far as hypoxia is concerned, Parati et al. [6] provided a comprehensive review of the relationship between hypoxia and cardiovascular disease. They discussed how hypoxia is a powerful moderator of cardiovascular function and how its effects are mediated by changes in autonomic

✉ Ligia Ferreira Gomes
lfgomes@usp.br

✉ Antonio Carlos Bloise
acbloise@usp.br

[1] Universidade de Sao Paulo, Instituto de Fisica, Rua do Matao 1371, Sao Paulo, Brazil

Published online: 18 March 2024

nervous system activity mediated by chemoreflexes, directly induced changes in vascular tone, and humoral changes, such as renin-angiotensin-aldosterone system suppression [6, 7]. Garcia Rojas et al. [8] described how hypoxia plays a central role in the pathogenesis and pathophysiology of all cardiovascular diseases and how the organism reacts to reduced oxygen availability. Compensatory mechanisms are mostly mediated by hypoxia-inducible factors (HIFs) and affect glucose transport, angiogenesis, handling of reactive oxygen species (ROS), cell proliferation, and survival. Recently, in vitro cell experiments have been used to evaluate the cellular activity of cardiomyocyte models in the hypoxia/reoxygenation process to determine whether the protective effect of diazoxide postconditioning on myocardial ischemia-reperfusion injury is related to the HIF-1/HRE pathway and whether ROS play a role in this process [9]. The authors found that diazoxide postconditioning stimulates the opening of the mitoK$_{ATP}$ channel to create a moderate ROS level, which activates the HIF-1/HRE pathway and causes myocardial protection [9].

Despite these important findings, the biological mechanisms underlying how hypoxia-reoxygenation can modulate immune cell functions in cardiovascular disease are poorly understood. In this context, the characterization of CMs' changed and basal metabolism through the identification of some fundamental metabolic pathways, such as glycolysis, TCA, and amino acid cycles, has recently emerged as a valuable tool in therapeutics [10–], especially in understanding cardiomyocyte activation and hypoxia-reoxygenation in cardiovascular disease. Here, we applied the HfR challenge (as defined before, "hypoxia followed by reoxygenation (HfR)") to non-proliferative CMs obtained from *wild type* neonatal rats [10] as an initial approach to characterize the biochemical transformations in the main anabolic and catabolic pathways, both quantitatively and qualitatively. To achieve this goal, we developed in our lab a special cell incubator able to produce hypoxia and normoxia conditions named from now on as "hypoxia incubator" or HI. CMs were then incubated using HI to produce stressed and non-stressed cells, harvested, and lyophilized to be used in this study. The CMs samples were analyzed using metabolomic based on proton magnetic resonance spectroscopy approach in order to characterize the metabolomes, endo- and exo-metabolome, of the challenged cells compared with regular cultivation cases and to identify the changed metabolic pathways. Here, the metabolism of CMs under HfR appears to yield an antioxidant cellular environment, which, in principle, could be used to balance the cardiac side effects of hypoxia or other traditional chemotherapeutic drugs. To our knowledge, our findings provide the first evidence of an adaptive cellular mechanism triggered by HfR procedure.

Materials and Methods

Cell Culture

Non-proliferative CMs were obtained from a pool of 10 to 15 neonate rat hearts, as described by [13] and [14] and were frozen in vials containing 2.0 to 2.5 millions of cells. The experimental procedures were performed according to the guidelines for ethical conduct used in animal care and were approved by the local institutional review board of the University of São Paulo Medical School, Brazil (#340/12). CMs were carefully thawed at room temperature by adding fresh culture media, previously warmed to 37 °C, and were subsequently seeded into 6-well cell culture plates with 9.5 cm^2 of surface area/well (Corning®, Darmstadt, Germany), allocating 580 ± 40 k cells for each well. The media used in these cultures was composed by a mixture of 4: 1 (V/V) DMEM (Dulbecco's Modified Eagle Medium low glucose, Gibco®, Waltham, Massachusetts, USA): M199 (Media 199, Gibco®) culture media supplemented with 1% (V/V) horse serum (HRS, Gibco®), 5% newborn calf serum (NBCS, Gibco®) and 1% bromodeoxyuridine (BrdU, Gibco®). The BrdU was used to prevent the development of non-cardiomyocyte cells.

In order to produce a controlled and reproducible in vitro HfR assay, two incubation conditions were defined. CMs were incubated at 37 °C, either in normoxia, referred as the basal condition when cells were incubated in an environment of 5% of CO_2 and 95% of filtered ambient air; or in the hypoxia condition when the cells were submitted to a continuous injection of N_2 gas inside the HI chamber, kepting the HI environment at negligible levels of the CO_2 mixture. Three experimental groups were defined: two basal groups (unstressed CMs) and one group undergoing HfR (stressed CMs). Unstressed CMs were split into two subgroups, respective of the equipment used in the experiments: a commercial CO_2-incubator (Series II Water Jacket, Thermo Scientific, Waltham, Massachusetts, USA), hereafter labeled CI; or the HI chamber, set to provide a normoxic environment. These subgroups were defined to provide an additional control of the experimental setting, confirming that the basal condition provided by the HI was equivalent to that provided by the commercially available equipment. The stressed CMs group, referred to as HfR, was exposed to the hypoxia-reoxygenation consecutive cycles by adjusting the timing as follows: 90 min for normoxia condition and 45 min for hypoxia, i.e., 135 min for one completed cycle which is repeated 45 times, totaling up 100 h *per* assay. This specific set of times was determined empirically based on estimates for cellular confluence obtained for a second lineage of cells used in this work: *rabbit aortic smooth* cells, RASM (please, address to "Supplementary Materials" for an overview of main

obtained results with this lineage of cells). In the result section we will go back to address shortly these assays with RASM cells.

Assays for the basal and HfR groups were performed in four sequential rounds of independent experiments. The usage mode of HI in basal or HfR conditions defined the specific set of experiments performed in each round as follows: *round-1* stands for HfR in HI and basal in CI, *round-2* stands for basal in HI and CI, *round-3* and *round-4* stand for repeats of *round-1* and *round-2*, respectively. The culture media samples were harvested twice: after 48 h, when cultures were replaced with fresh media, and after 96 h. Cell samples were harvested only once: at the end of entire culture rounds, after 96 h.

Resonance Samples Preparation

To ensure the purity of media samples, the entire content of each well was transferred to 15 mL tubes, centrifuged for 10 min at 110 g at room temperature. Aliquots of 2 ml of supernatant were then collected, transferred to lyophilization vials, frozen at −80 °C and stored between two, and no more than 4 weeks, posteriorly they were thawed at room temperature for ~5 min and immediately transferred to a lyophilizer to be lyophilized for 24 h. Meanwhile, cells were harvested by trypsinization [15], manually counted in the Neubauer hemocytometer and processed for metabolic extraction [10, 11, 16, 17]. Cell lysis and extraction was performed in an Bandelin *Sonoplus* ultrasound device, model GM 2070 of 70 W (Merck®), with 1 ml of cold methanol-water mixture (1:1), through six treatment cycles of 30 s pulses (50–60% of power) plus 5 min intervals. The obtained suspensions were then centrifuged in 2 ml microcentrifuge tubes for 90 min at 310 g at 4 °C to sediment cell debris. Supernatants were collected, aliquoted (~850 µL), frozen at −80 °C and manipulated in the same manner of media samples in order to be lyophilized for 24 h. The lyophilized extracts, media, and cells were diluted in 650 µL of deuterium oxide (D_2O, Sigma-Aldrich®, Darmstadt, Germany) containing 4,4-dimethyl-4-silapentane-1-sulfonic acid (DSS, Sigma-Aldrich®) at, respectively, 5.0 mM for culture media and 0.5 mM for cellular extracts, and finally transferred into 5 mm resonance tubes, immediately prior to the resonance experiments.

Metabolomics and Resonance Spectroscopy

The effects of HfR on CMs metabolism were evaluated using metabolomics based on high-resolution proton magnetic resonance spectroscopy (^{1}H-MRS) approach through the acquisition of multiple spectra from liquid samples of cellular extracts and culture media. These spectra were representative of the two groups of cells incubated in basal normoxic conditions and one group of cells submitted to the HfR treatment. Individual analytical samples of cells and media culture were identified by an acronym composed by letters and numbers in the format "XXy##", in which the first to digits were associated to the incubation condition (HR or BL, for HfR or basal condition), the third digit indicates the incubator used (h or c, for HI or CI) and, for culture media samples only, the last two digits indicate the total incubation time at the moment of harvesting, in hours (48 or 96). The cell samples acronyms were composed only by letters, because all cell samples were collected after 96 h. It's worth clarifying that we had some issues during the cell's cultivation which resulted in an imbalance of the number of replicates *per* group, varying between 5 up to 9 replicates depending on the experimental situation faced in the day of cell manipulation. For instance, we lost two wells containing CMs from the BLh group. Besides, in the rounds 2, 3, and 4 of the cells cultivated in CI, we had to reduce the number of replicates to only one due the lower amount of CMs present in the corresponding frozen vials of these rounds. Thus, at the end of the four rounds, we evaluated 16 cellular extracts (6 HRh, 5 BLh, and 5 BLc) and 42 culture media samples (6 HRh48, 6 BLh48, 9 BLc48, 6 HRh96, 6 BLh96, and 9 BLc96) as shown in Fig. 1.

The ^{1}H-MRS experiments were performed in a Varian spectrometer (Varian Inc., Palo Alto, California, USA) with three channels and pulsed field gradients, coupled to 5 mm triple resonance probe (^{1}H, ^{13}C, ^{15}N) operating at constant frequency of 399.7 MHz for protons nuclei. Spectra were conveniently acquired using a combination of the NOESY-1D pulse sequence and selective saturation of residual water. Some experimental conditions were kept constant between the acquisitions of cellular extracts and culture media: temperature of 25 °C, spinning rate of 20 Hz, relaxation delay of 1.0 s, excitation pulse of 7.5 µs wide, mixture time of 150 ms, and selective water saturation pulse of 2.0 s wide applied at ~4.7 ppm respect to DSS. For the cell samples, a spectral window of 10 ppm, 32 Kbytes data points, and 3000 transients *per* signal (~3 h of acquisition) were used. For culture media samples, a spectral window of 12 ppm, 64 Kbytes data points, and 192 transients *per* signal (~20 min of acquisition) were used. A weighted Fourier transformation with a line broadening of 0.3 Hz was applied to all spectra (cells and media), followed by phase adjustment and baseline correction through spline curves. Magnetic field homogenization through shimming procedures was performed before each acquisition to ensure a reasonable spectral resolution, and the values for the line width at half height of the DSS, which varied from 0.5 to 1.5 Hz. Additionally, the calculus of signal-to-noise ratios (SNRs) was used to determine the level of uncertainty in our measurements. Spectra showed values that varied from 40 to 200 for cells and 800 to 5000 for culture media

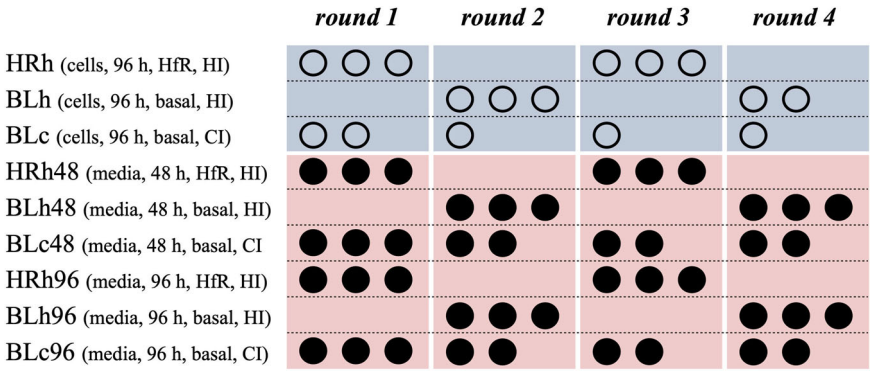

Fig. 1 Summary of the resonance samples obtained from CMs cultures at the end of each of the four 96 h incubation rounds. The nomenclature used in this work considers, respectively, type of sample (cells or media), incubation time (48 h or 96 h), incubation condition (basal or HfR), and incubator device (HI or CI) as follows. "HRh": (cells, 96 h, HfR, HI); "BLh": (cells, 96 h, basal, HI); "BLc": (cells, 96 h, basal, CI); "HRh48" and "HRh96": (media, 48 h and 96 h, HfR, HI); "BLh48" and "BLh96": (media, 48 h and 96 h, basal, HI); and "BLc48" and "BLc96": (media, 48 h and 96 h, basal, CI). Throughout this cultivation strategy, we generate the nine groups of this study each one composed by replicates of resonance samples as indicated to the open circles for cells, or cellular extracts, and solid circles for media, or culture media. The imbalance in the number of replicates *per* group was attributed to some experimental issues as described before in this section

resulting, on average, SNRs of 145.7 ± 92.9 and 2453.1 ± 1866.3 respectively for cells and media.

Statistics Data Processing

In metabolomics, all statistical processing should be performed by taking preventive actions regarding the normalization of spectroscopic data to avoid misinterpretations of generated results. This work used two methods of normalization. First, chemical shifts x-axis was adjusted placing the DSS signal to 0 ppm and rescaling the y-axis upon correlating the DSS area to the correspondent concentration of this molecule in the samples, i.e., 0.5 mM for cellular extracts and 5.0 mM for culture media. The second spectral normalization applied for cells and media samples was carried out performing the computation of total area of their respective spectra between 0.7 and 8.6 ppm, discounting the interval of residual water signal between 4.2 and 5.5 ppm, and dividing their intensities by the corrected areas. These actions prevent, respectively, issues regarding alterations in sample pH that could shift the high-resolution lines and slight alterations in the resonance spectrometer gain that could distort the signal intensities (first normalization), and changes in the lyophilized mass of cells or culture media components variability that could influence the composition of metabolite areas in the spectra (second normalization) [10–12, 16–18]. A third data normalization was also applied, in the multivariate statistical method used by this work, the "Partial Least Squares-Discriminant Analysis" (PLS) [19, 20]. This normalization consists of rescaling all input variables of the method, the metabolites areas, by mean-centering and dividing each area by its corresponding standard deviation, thus preventing imprecise results resulting from large differences among their magnitudes. The assignments of high-resolution peaks and their respectives quantification were all performed using a commercial license of *Chenomx* NMR Suite software (©Copyright 2009 - 2024 Chenomx Inc., Edmonton, Alberta, Canada).

PLS was performed using SIMCA-P+ software (Umetrics^{TM}, Malmö, Sweden), rescaling input variables as described, four components in the model for both computing predictions and displaying results, seven steps of cross-validation groups, 95% confidence level of parameters, and 0.05 for significance level of Hotelling's T2 ellipses [21]. In this statistical method, any group of similar samples, cells or culture media under basal or HfR conditions, could be observed in a bi-dimensional plane, and classification variables responsible for the observable grouping (metabolite areas) were ranked as "Variable of Importance in Projection" (VIPs) in descending order. VIPs that showed values greater than 1 [22] were retained for further analysis of their respective statistical relevance. The last test was carried out using either a parametric univariate t-test or a nonparametric Kruskal-Wallis test suitable for comparisons of two different sample groups. Data normality was previously checked using the Anderson-Darling test [23]. All analyses were performed using *Minitab* (Minitab Inc., institutional license, State College, Pennsylvania) with a confidence level of 95%.

Statistical comparisons performed in this study, multi- and univariate, revealed the characteristic metabolic profile differences of CMs under basal and HfR conditions after 96 h of incubation as directly evaluated through the cells' metabolites. Also, the corresponding dynamic evolution of the metabolic changes was indirectly evaluated with the

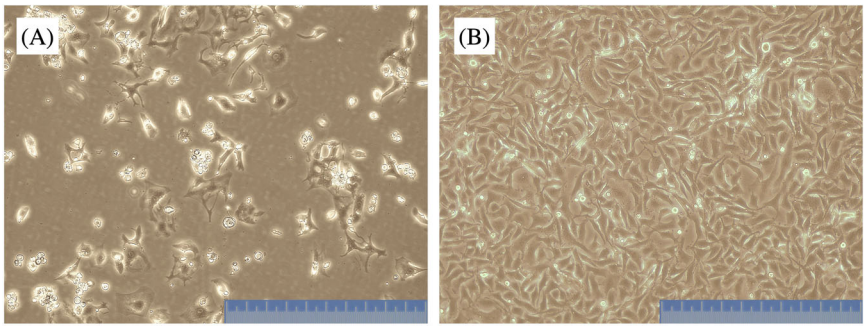

Fig. 2 Microscopy images (10x) showing CMs morphological and confluence aspects after 48 h of HfR treatment or stressed CM (**A**) and basal state or unstressed CMs (**B**) at same incubation time. Scale bars: 0-1 mm/100

culture media collected after 48 h and 96 h. The comparisons regarding the performance of HI were included in the supplementary materials, in order to add robustness to the obtained results. Summarizing, eight cases of comparisons will be discussed: (1) [HRh vs. BLh] for evaluation of 96 h of the HfR treatment on cell samples, (2) [BLh vs. BLc] for evaluation of 96 h of the basal-performance in HI on cell samples, (3) [BLh48 vs. BLh96] for evaluation of the basal time evolution of media samples obtained in HI, (4) [HRh48 vs. HRh96] for evaluation of the dynamic of HfR treatment on media samples, (5) [BLh48 vs. HRh48] and (6) [BLh96 vs. HRh96] for evaluation of the HfR treatment at, respectively, 48 h and 96 h on media samples, and (7) [BLh48 vs. BLc48] and (8) [BLh96 vs. BLc96] for evaluation of the basal-performance in HI at, respectively, 48 h and 96 h on media samples.

Results

In this work, homeostatic mechanisms triggered by neonatal cardiomyocytes obtained from rats due to the stress associated with HfR were detected in the regular catabolic/anabolic pathways through ^{1}H-MRS-based metabolomics. To fulfill this goal, an incubator able to induce cellular hypoxia was designed and built to promote HfR, and its basic functionalities were checked and previously certified. The incubator prototype was able to provide stable temperature and humidity in the internal chamber and to support endothelial and muscular lineage cells growth without contaminations for several passages. However, HI was less effective in culture media buffering than the commercial equipment. In fact, hired commercial certification tests revealed that the CO_2 levels in HI were ~60% of the levels found in CI. The impact on the pH of culture media free of cells incubated for the same period of time (48 h) was evaluated, and the obtained final pH results were: 8.20 ± 0.04 in HI versus 7.80 ± 0.06 CI. In order to refine the metabolic analysis of the HfR effects on CMs, this study managed to separate any metabolic contribution to CMs due to pH variation and included the comparison of the metabolic effects of two groups of controls, cultivated in HI and CI in putative equivalent conditions.

The first point that we should address in this section concerns the set of times used to induce the stressed CMs. As mentioned before, we determined empirically through estimates for cellular confluence with RASM cells assays that we performed before the main experiments with CMs. For instance, we obtained ~60% for RASM confluence at the end of 48 h of HfR treatment using 60 min in normoxia condition and 120 min in hypoxia equivalent to 180 min for one completed cycle which was repeated 16 times to complete 48 h. Thus, we assume that due to the fragility of primary CMs lineage when compared to immortalized RASM lineage, in order to prevent excessive cellular death of cardiomyocytes, the hypoxia and normoxia times should be exchanged, reducing the hypoxia period and increasing the normoxia. In Fig. 2A we show the stressed CMs confluences reached at the end of the first 48 h estimated between 40% and no more than 50% using this new set of times presented in the material and methods section, while in Fig. 2B, we show the case of unstressed CMs with confluence nearly at 100%. Additionally, Neubauer chamber countering also demonstrated the fragility of CMs lineage with expected reductions of their respectively average values calculated from countering of 6 individual wells seeded, each one, with 580 k cells: 362 ± 198 k at basal and 62 ± 47 k to CMs under HfR, a reduction of ~80% between the two results. Increasing the treatment period of time, the preconditioned CMs number changes to 76 ± 37 k at the end of 72 h, quite similar to previous time upon considering the standard deviation, and 24 ± 9 k at the end of 96 h indicating an expressive reduction.

Table 1 summarizes the results obtained using this analytical procedure. In this table, identified metabolites and their respective synonyms are presented in the first and second columns, and chemical shifts are shown in the third column as positions of higher intensity lines for both cellular extracts (Fig. 3, BLh and HRh spectra) and culture media samples (Fig. 3, BLh96 and HRh96 spectra). Through line-shaping fitting of individual lines, normalized areas corresponding to relative concentrations of

Table 1 ^{1}H-MRS chemical shift assignments obtained in spectral analysis of *cellular extracts* and *culture media* samples

Metabolites	Synonyms	Chemical Shifts (ppm)	
		cellular extracts	culture media
Leucine	[a]Leu	0.80	0.9; 1.0; 1.2; 1.5; 2.0; 3.7
Isoleucine	[a]Ileu	0.83	0.9; 1.0; 1.7; 3.7
Valine	[a]Val	0.96	1.0; 2.3; 3.6
Ethanol	EtOH	–	1.2; 3.6
Threonine	[a]Thr	–	1.3; 3.6; 4.3
Lactate	Lac	1.31	1.3; 4.1
Alanine	Ala	–	1.5; 3.8
Cadaverine	DAPE	–	1.5; 1.7; 3.0
Arginine	[a]Arg	–	1.6; 1.7; 1.9; 3.2; 3.8; 6.7; 7.2
Acetate	AcOH	1.90	1.9
Pyroglutamate	Pyro	–	2.0; 2.4; 2.5; 4.2; 7.7
Methionine	[a]Met	–	2.1; 2.2; 2.6; 3.9
Acetone	–	2.21	2.2
Succinate	e363	–	2.4
Pyruvate	BTS	–	2.4
Dimethylamine	DMA	–	2.7
Tyrosine	[a]Tyr	–	3.0; 3.2; 3.9; 6.9; 7.2
Methanol	MeOH	3.34	–
Glycerol	Gro	3.54	–
τ-Methylhistidine	3-MHis	–	3.1; 3.2; 3.7; 4.0; 7.0; 7.7
Phenylalanine	[a]Phe	6.90	3.1; 3.3; 4.0; 7.3; 7.4
Glucose	[a]GLC	–	3.2; 3.4; 3.5; 3.7; 3.8; 3.9; 4.6; 5.2
Nicotinurate	–	–	4.0; 7.6; 8.2; 8.7; 8.8; 8.9
Formate	Add-F	8.44	8.4

Short names (synonyms) are shown in agreement with The Human Metabolome Database (HMDB). Assignments referenced through 4,4-dimethyl-4-silapentane-1-sulfonic acid, DSS (-CH_3-)$_3$, line at 0 ppm

[a]Originally present in culture media composition

metabolites or metabolite levels were obtained and used in statistical analysis to probe the response to HfR effects on the endometabolome and exometabolome of cells [11, 12], as will be discussed further.

Plots in Fig. 4A–F, summarize the results obtained from the PLS analysis of the first 6 cases of group comparisons proposed in the material and methods section. Dual comparisons between the groups were used to evaluate the following situations: CMs metabolism changes attributable to HfR (Fig. 4A); HI performance for basal condition cultures (Fig. 4B); dynamic effects upon culture media obtained from CMs kept under basal (Fig. 4C) and HfR (Fig. 4D) environments; and effects of HfR upon CMs metabolism that were reflected in culture media composition after 48 h (Fig. 4E) and 96 h (Fig. 4F). Plots in figures were complemented by estimates for R2Y and Q2, respectively, accuracy of variable variation and predictability (estimated by cross-validation) of the variable ability to predict the assertiveness of generated results [21].

As can be seen in Fig. 4, there were clustering tendencies for all studied cases. For instance, the HfR effect evaluated over 96 h of CMs metabolism could be readily identified by comparison with CMs at basal conditions as indicated, respectively, by the set of red squares in the up-down right quadrants (HRh group) and the set of blue dots in the up-down left quadrants (BLh group) in Fig. 4A. The observed changes in the metabolite's levels profile were produced by changes in the metabolism of cells. Then, the metabolite level changes were evaluated from the analysis of the corresponding VIPs and checked for their respective statistical significance through univariate tests for dual comparisons to identify quantitative changes in their levels. The obtained *landmark metabolites* (l.m.) were referred in further discussions as "cell's HfR metabolites" or, simply, "{cHR}". Also, the analysis of cell samples identified and excluded effects due to differences in performance between HI and CI, which was considered the standard for cell incubation conditions. For this purpose, PLS analysis was performed on the BLh and BLc groups, as shown in Fig. 4B.

A slight separation between the dispersion centers of points was observed, disclosing the presence of discriminant metabolites for this case. The contributions from each identified metabolite to {cHR} associated changes were verified using *t*-test for normal data distributions or Kruskal-Wallis for non-normal distributions of the corresponding VIPs, as summarized in Fig. 5A and Supplementary Materials, Supplementary Table S1. Contributions were then quantified as *percentage increment rates* calculated from the expression $100 \times [(met_A - met_B)/met_A]$, where met_A is the metabolite area, or median for non-normal distribution data points, of the first compared group, and met_B is the metabolite area (or median) of the second compared group, results are presented in Table 2, fourth column. For example, leucine and isoleucine, {cHR} metabolites, had their levels increased by 37.2 and 44.7%, respectively, whereas phenylalanine decreased by 83.2%, highlighting ketogenic aminoacid catabolism. In addition, practically no detectable levels of lactate, a flag metabolite of cell anaerobic metabolism [24], were observed in the {cHR} condition. Incubation time effects complemented the metabolomic analysis by providing numeric parameters addressing the evolution of the levels of these metabolites, enabling systematized comparisons of HfR time effects.

The PLS results obtained from the culture media showed clustering tendencies for the dynamic evolution of the metabolic profile in both BL and HR groups (Fig. 4C, D),

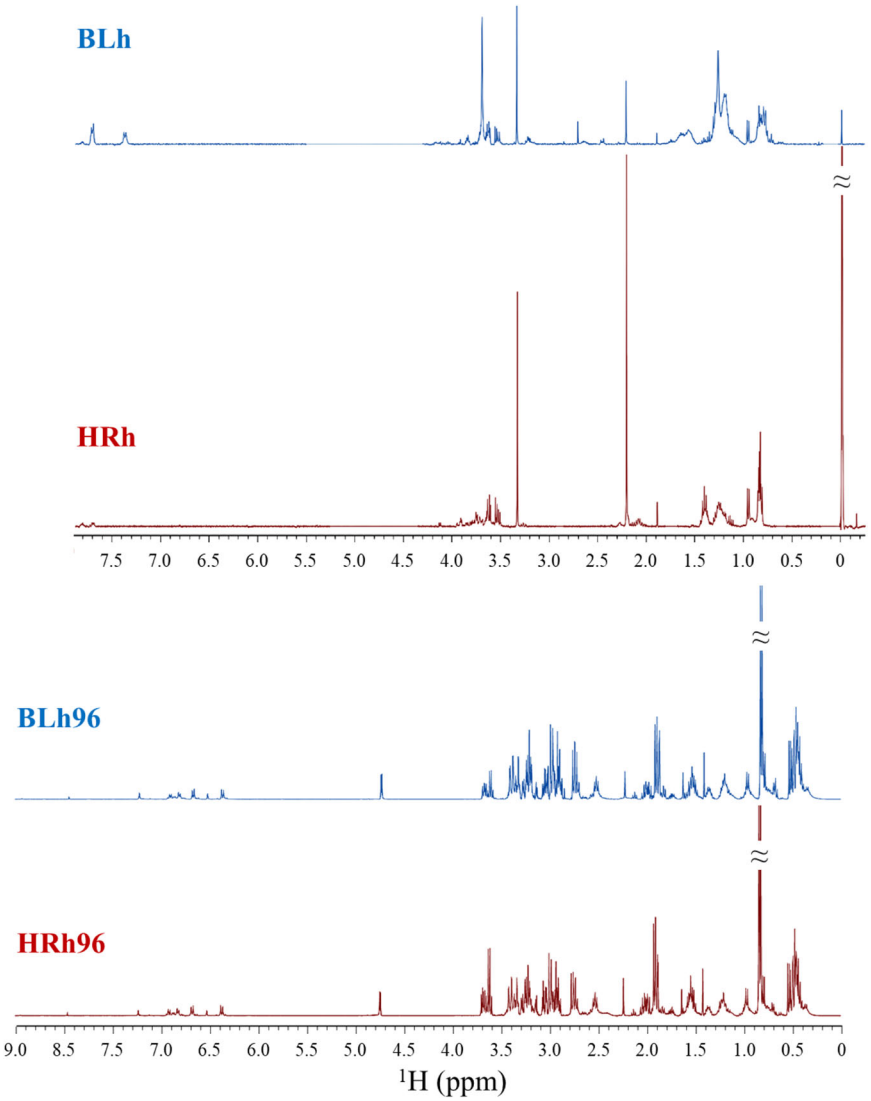

Fig. 3 High-resolution spectra obtained at 399.7 MHz and 25 °C of cellular extracts and culture media samples, respectively, under basal (BLh and BLh96, blue) and HfR (HRh and HRh96, red) conditions after 96 h of culture in HI. The water signal present in spectra between 4.2 and 5.5 ppm and the DSS reference-singlet at 0 ppm were suppressed just for a clarity view of metabolites lines. These spectra have their own common y-scales allowing direct comparisons among lines of cellular extracts or culture media, but not between them due to the low SNRs values reached in the first one that were almost twenty times lower, thus they were proportionally stretched to be visible in the scale of the last one. Spectral line identifications for both sample types are summarized in Table 1

when comparing the 48 h and 96 h samples. It was assumed that these results may reflect the metabolites profile generated from changes in the cell metabolism that may include contribution of cell damage and death. The landmark metabolites identified in the culture media, using the same analytical procedure applied to CMs, were associated to the dynamics of basal and HfR and named, respectively, as "media's Dynamic Basal metabolites", or "{mDB}", and "media's Dynamic HfR metabolites", or "{mDHR}". These results also considered the identification of the metabolites produced due to issues of performance of HI that could interfere with the basal state time evolution of CMs cultivated in our device. Then, profile changes identified after the statistical analysis of the comparison [BLc48 vs. BLc96], were removed from mDB, as summarized in Fig. 5B and Supplementary Materials in the Supplementary Table S1, showing [BLc48 vs. BLc96] comparison, and in Supplementary Fig. S2A, showing scores plot. Finally, the set obtained for mDB and those referred to the performance of HI were used to identify and exclude dynamic effects that couldn't be unequivocally attributed to HfR treatment, because they were also identified in one of the basal conditions either in CI or HI. Then, the mDHR could be associated with the dynamics of HfR treatment. This analysis is summarized in Fig. 5C.

The PLS results on culture media effects revealed that they were more intense in the first 48 h than between 48 h and 96 h. The clustering of data, and the high values of R2Y and Q2 indicate that the HfR effects were accurate and assertive (Fig. 4E). To complete this analysis, VIPs results were also statistically processed and the obtained l.m. isolated by time of HfR event were named as "media's time Persistent HfR metabolites-hh", or "{mPHR-hh}" (hh = 48 h and 96 h). A subsequent analysis to exclude the contribution of metabolites that came out exclusively due to the difference in performance between HI and CI and were

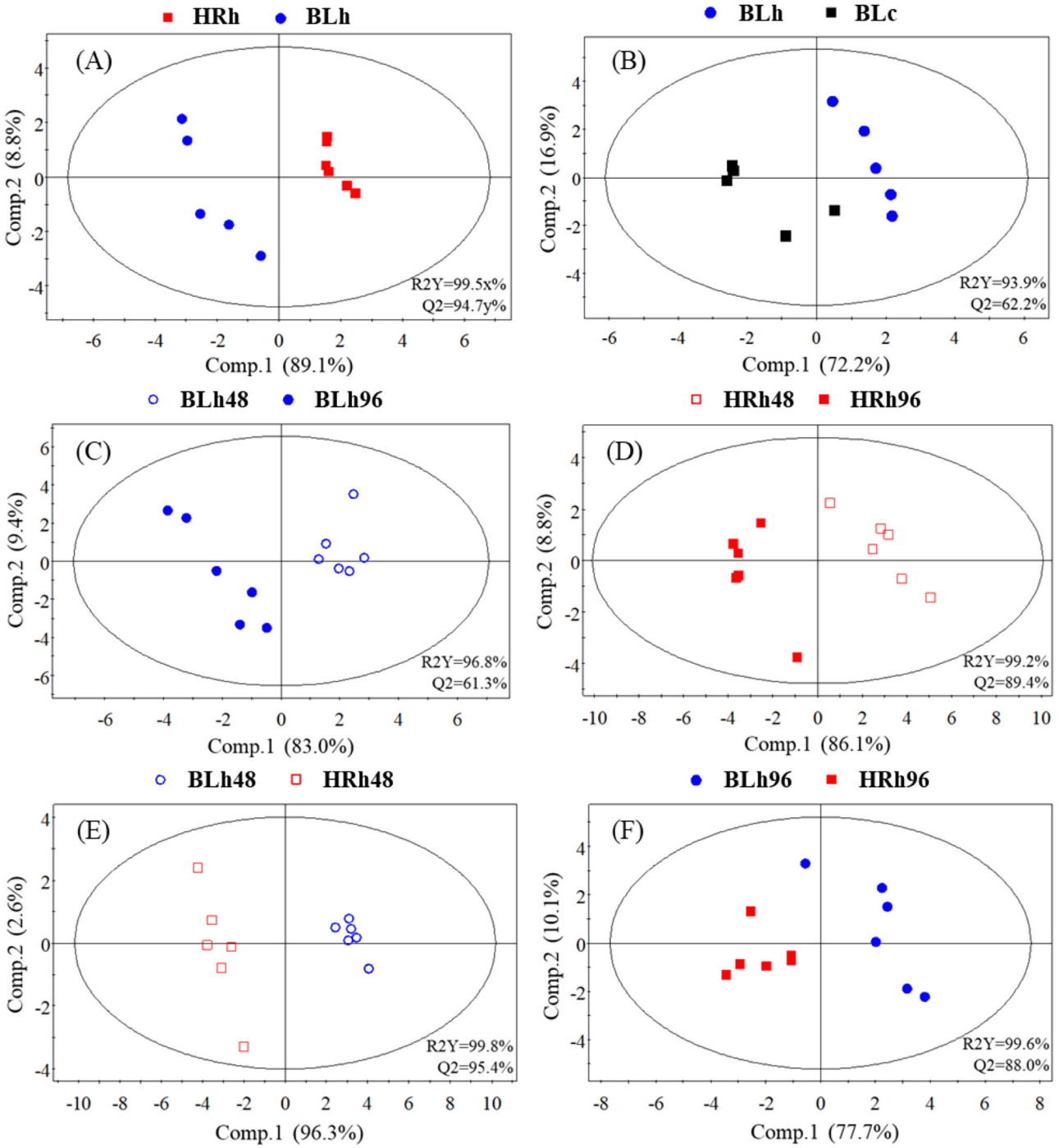

Fig. 4 Overall summary of PLS bi-dimensional scores plot generated using spectral data of cellular extracts and culture media samples acquired from lyophilized samples produced by cells in different culture conditions, synthesized by dual-comparisons: (**A**) [HRh vs. BLh], and (**B**) [BLh vs. BLc] corresponding to cell samples labeled as red boxes for the HRh group, blue dots for the BLh group, and black boxes for the BLc group; (**C**) BLh48 vs. BLh96; (**D**) HRh48 vs. HRh96; (**E**) BLh48 vs. HRh48; and (**F**) BLh96 vs. HRh96 corresponding to media samples labeled as blue circles for the BLh48 group, blue dots for the BLh96 group, red squares for the HRh48 group, and red boxes for the HRh96 group. Brackets show the percentage (%) of explained data variance and the values obtained for R2Y and Q2; tolerance ellipses were based on Hotelling's T2

detected in media samples was performed, in analogy to the previous analyses. Comparisons of BLc48 vs. BLh48 and BLc96 vs. BLh96, summarized in Supplementary Materials in Supplementary Table S1 and Supplementary Figure S2B, C, address this analysis. As expected, the PLS score plots of this supplementary figure showed some degree of

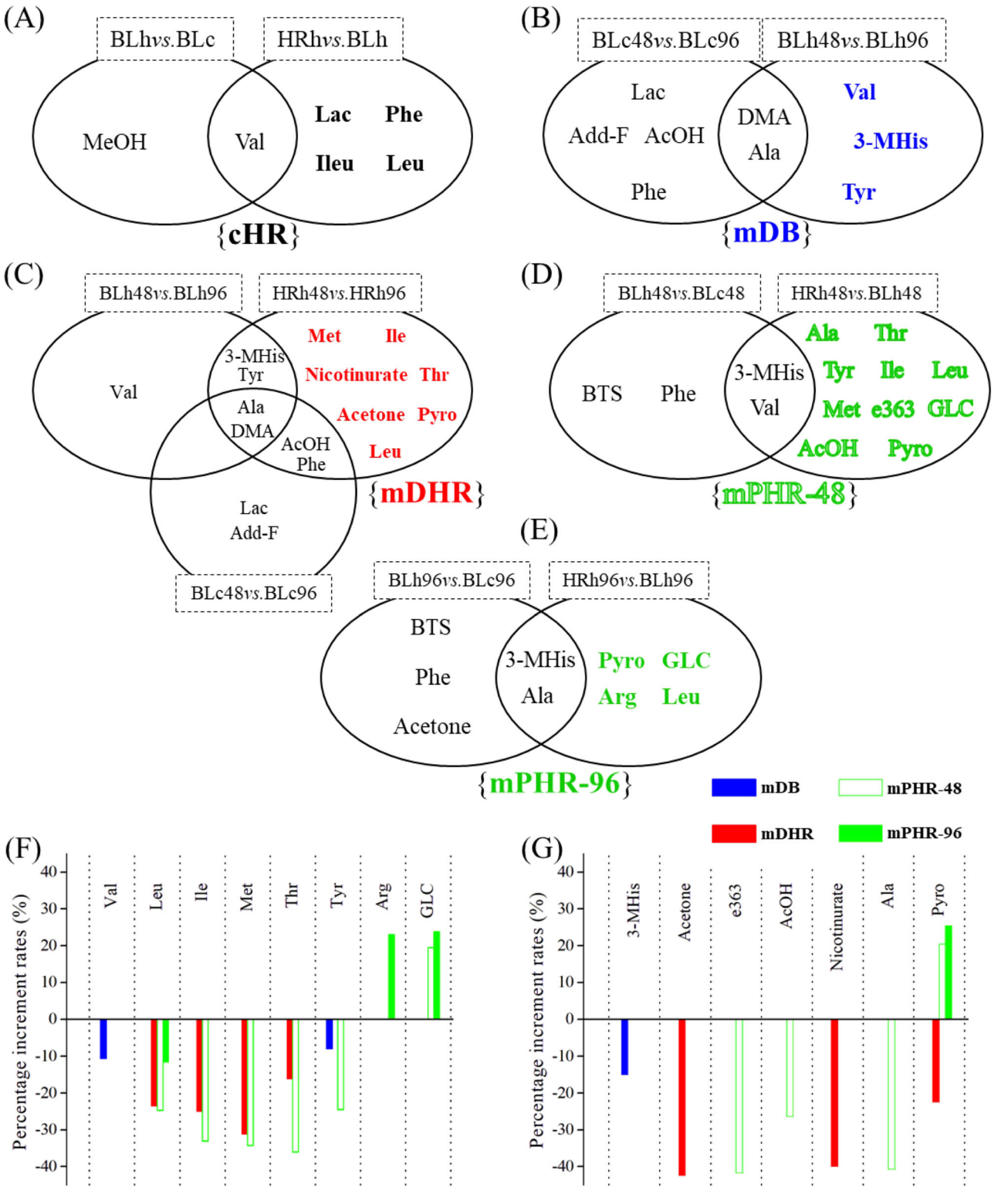

Fig. 5 The classification of landmark metabolites (l.m.) was generated when basal and performance effects were excluded from statistical analysis, illustrated through concepts of topological space. Key: (**A**) {cHR} for "cell's HfR metabolites"; (**B**) {mDB} for "media's Dynamic Basal metabolites"; (**C**) {mDHR} for "media's Dynamic HfR metabolites"; {mPHR-hh} for "media's time Persistent HfR metabolites at (**D**) 48 h and (**E**) 96 h" and percentage increments associated with the l.m., described in terms of (**F**) consumed and (**G**) excreted components by CMs on culture media samples exhibited as bar graphics plots

Table 2 Statistical analysis summary showing compared cases (first column), obtained *VIPs* in descendent order (second column), *p* values resultant from *t*-test or Kruskal-Wallis analysis (third column), and percentage increments rates of landmark metabolites for $p < 0.05$, calculated from $100 \times [(met_A - met_B)/met_A]$, where met_A is the *met*abolite area, or median for non-normal distribution data points, of first compared group and met_B is the *met*abolite area (or median), of second compared group: positive values of this rate mean increasing for "A" group while negative values means decreasing (fourth column)

Groups comparisons: [A vs. B]	VIPs (≥1)	*p* values	Percentage increment rates (%)
[HRh *vs*. BLh] *four days evaluation of CMs undergoing HfR treatment on cellular extracts*	Phe	0.001	−83.2
	[a]Lac	0.028	$<10^{-10}$
	Val	0.008	59.1
	Ileu	0.016	44.7
	Leu	0.039	37.2
[BLh48 *vs*. BLh96] *dynamic evaluation of basal CMs on culture media*	[a]DMA	0.004	97.3
	Val	0.001	−10.5
	Ala	0.003	−17.3
	3-MHis	0.005	−15.0
	Leu	0.070	–
	[a]Lac	0.055	–
	[a]Tyr	0.013	−7.9
[HRh48 *vs*. HRh96] *dynamic evaluation of CMs undergoing HfR treatment on culture media*	[a]DMA	0.004	97.7
	Phe	<0.001	−23.6
	Tyr	<0.001	−28.1
	Acetone	0.002	−42.4
	3-MHis	0.001	−20.7
	Met	0.002	−31.1
	AcOH	0.002	−23.2
	Ile	0.003	−24.9
	[a]Nicotinurate	0.020	−40.0
	Pyro	0.004	−22.5
	Leu	0.008	−23.4
	[a]Ala	0.010	−34.6
	Thr	0.029	−16.1
[HRh48 *vs*. BLh48] *evaluation of CMs undergoing HfR treatment on culture media collected with two days from day zero*	[a]Ala	0.004	−40.8
	Thr	<0.001	−36.0
	Tyr	<0.001	−24.6
	Val	<0.001	−29.5
	Met	<0.001	−34.2
	Ile	<0.001	−33.1
	e363	<0.001	−41.8
	[a]Pyro	0.010	20.4
	3-MHis	0.001	−25.3
	AcOH	0.005	−26.3
	Leu	0.009	−24.8
	Thr	0.029	−16.1
	GLC	0.017	19.4
	3-MHis	<0.001	−19.3
[HRh96 *vs*. BLh96] *evaluation of CMs undergoing HfR treatment on culture media collected with four days from day zero*	Pyro	0.004	25.4
	GLC	0.012	23.8
	Ala	0.011	−26.5
	e363	0.059	–
	Arg	0.035	23.0
	Leu	0.031	−11.5
	DMA	0.108	–
	Ile	0.067	–
	[a]EtOH	0.078	–

Results obtained for both types of samples, *cellular extracts*, and *culture media*

[a]Non-normal data distribution, *t*-test was changed by Kruskal-Wallis and median values used in this case

separation between the cell groups incubated in normoxia in CI and HI, but with higher proximity between the centers of point distribution and dispersion of points, as well as low assertiveness parameters when compared with the experimental comparisons involving HfR effects. This behavior confirmed the low impact of the performance differences of incubators upon CMs metabolism. Finally, Fig. 5D, E summarizes, respectively, the resultant set obtained for {mPHR-48} and {mPHR-96}, respectively. The first 48 h period showed an increased consumption of [§]{mPHR-48} leucine, isoleucine, methionine, threonine, and tyrosine (Fig. 5F) and a decreased excretion of succinate, acetate, and alanine (Fig. 5G). There was also an increase in the concentration of pyroglutamate in the media conditioned by the stressed CMs (Fig. 5G). Most of these changes were not observed or were less expressive in the 48 to 96 h period than during the 0 to 48 h period, except for the excretion rate of pyroglutamate as shown in Fig. 5G. Pyroglutamate excretion was consistently increased in both samples by 20.4% (48 h) and 25.4% (96 h), implying metabolic shift towards adaptive mechanism and antioxidant protection.

To provide a better view of how the l.m. levels change in culture media samples in relation to the time span of the exposure to the environmental challenge, Fig. 5 also presents the results obtained for the percentage increment rates using bar graphics plots representation, taking into account two cases: metabolites that were *consumed*, covered by Fig. 5F, and *excreted*, as shown in Fig. 5G. It was observed that over the first 48 h interval of CMs in culture, at basal conditions, the levels of valine and tyrosine in Fig. 5F, and τ-methylhistidine (3HMis) in Fig. 5G have decreased in the media when compared with the subsequent 48 h of culture by 10.5, 7.9, and 15.0%, respectively. It is worth remembering that, as all metabolites labeled by the "§" symbol in

Table 1, valine and tyrosine are components originally present in the culture media composition; thus, their decrease in these samples can be interpreted as an increase in their consumption by cells at approximately the same rate. 3HMis is a metabolite that did not previously exist in the media composition and is thus excreted by cells. The resulting metabolic profiles shows specifically the main metabolites that can discriminate HfR effects that were different between the 48 h and 96 h cultures and how their levels are evolving. An analogous tendency of increase in the consumption of §{mDHR} by stressed CMs was also observed for the first 48 h for the metabolites leucine, isoleucine, methionine, and threonine, respectively, in 23.4, 24.9, 31.1, and 16.1%, respectively, compared with the last 48 h of cell culture (Fig. 5F). Acetone, pyroglutamate, and nicotinurate, metabolites showed 42.4, 22.6, and 40.0% reduction in their excretion rates, respectively (Fig. 5G). These results support the early induction of a metabolic change towards ketogenic metabolism in the first period, followed by CMs selection and extensive death.

Discussion

In this study, a metabolomic approach using ^{1}H-MRS as a spectroscopic tool was applied to investigate CMs obtained from neonatal rats and subjected to cellular stress in an in vitro model for HfR challenge. To make this study feasible, it was designed, built, tested, and used in our laboratory, an operational prototype of a homemade incubator using only cheap materials such as microcontrollers and 3d printable pieces that could also be replicated in other laboratories. Although this homemade incubator was previously tested and displayed a well documented acceptable performance in support of commercially available endothelial cells viability and growth, it presents a less effective CO_2 dependent buffering. Then, this study included two independent control groups, one dedicated to disclose the hypoxia effects upon the metabolism of the challenged cardiomyocytes respective to its unexposed controls and the other, to identify any interference attributable to the lower buffering performance of the equipment.

The analysis of cellular extracts and culture media samples, respectively, provided the endo- and exometabolomes of cells [10–12, 16–18]. The global metabolism of cells could be characterized by the endo- and exometabolomes generated by metabolomics and the differential results were associated with the environmental challenges, thus providing qualitative evidence about how stressed cells regulate their internal mechanisms in such extreme conditions. Despite the complexity of the information generated through metabolomics, it was proposed a reasonable strategy for isolating the metabolic effects, in terms of the five main comparisons summarized in Fig. 4A–F. The major results obtained are shown in Fig. 5A–E, addressing the qualitative aspects of the metabolomes in each analyzed case (Fig. 5F, G, and Table 2). The biochemical profiles allowed an expanded overview of how these CMs evolved over time under the stress induced in vitro by HfR cycles and its relationship with the homeostatic mechanisms triggered by cells.

The first issue to be discussed concerns the results obtained in the cell samples regarding the set of all l.m. obtained in the analysis of HfR events, named before as {cHR}. Due to the sample preparation method used in this study, these molecules were produced from cell lysis and active dissolution of macromolecular components, then {cHR} elements were assumed to originate from living cells. As expected, stressed cells have, on average, less oxygen available than basal cells, which could impact the chain of oxidative events of TCA at different points, forcing them to seek alternative routes of synthesis to meet their needs for energetic substrates while regulating intermediate concentrations in order to keep the cycle running appropriately. The stressed CMs presented an increase in their contents of leucine and isoleucine and a decrease in their contents of phenylalanine, respectively to normal cells. This metabolic pattern indicates how stressed CMs adapted their energetic metabolism, involving the converged biosynthesis of acetyl-CoA and the input of TCA intermediates from cytosolic aminoacids supplies after the HfR event. Alanine was previously shown to increase in cardiomyocytes during hypoxia. In this work, as alanine levels were different between the homemade and commercial equipment, then it would not be considered among the {mDHR}. The aminoacids leucine, isoleucine, and phenylalanine can converge through protein catabolism into the acetyl-CoA, an input substrate of TCA cycle (citrate cycle, Krebs cycle) [25]. Indeed, leucine is an exclusive ketogenic aminoacid, while isoleucine can converge to succinyl-CoA, but phenylalanine can converge to fumarate, another intermediate component of TCA cycle. The obtained profile suggests that stressed CMs increased protein degradation in order to provide an increase in the TCA pathway intermediates required to optimize the ketogenic anaerobic metabolism [25]. Autophagic behavior was probably triggered by extreme conditions, but the culture media profiles obtained for {mPHR-48} and {mPHR-96} indicate that the cells succeeded in activating both succinate accumulation signaling and antioxidant protection. The aminotransferase anaplerosis and glycolysis were demonstrated by Zhang and collaborators as the main source of succinate in cardiomyocytes and heart tissues under hypoxia [26]. These were probably the main mechanisms triggered by the HfR conditions, improving the energy production by the CMs during hypoxia, but also increasing the reoxygenation associated with cell damage.

Lactate is a monocarboxylic acid excreted by animal cells during lactic fermentation from the reduction of pyruvate molecule, catalyzed by lactate dehydrogenase, through coenzyme NADH oxidation [25, 27], which play an important role in signalizing anaerobic processes [24]. Our results showed that incubator performance didn't change cell concentrations of lactate; therefore, we classified this metabolite as {cHR} (Fig. 5A). This finding suggests that stressed CMs can auto-regulate themselves to cope with cycles of hypoxia stress upon driving their main ways of energy production towards TCA, and that oxidative phosphorylation pathways were relevant during reoxygenation, improving energetic balance [28]. The observed reduction in lactate excretion also indicates less anaerobic cell metabolism [24] in stressed CMs, probably due to the HfR cycling conditions, that allows lactate and succinate consumption during the first minutes of reoxygenation.

Regarding the results found in the media samples, these are summarized by the four main comparisons shown in Table 2 and three complementary ones shown in Supplementary Materials (Supplementary Table S1). It is worth noting that in these samples, we probed molecules that were consumed by cells as essential nutritional elements originally present in commercial culture media, but also molecules that were excreted as a result of their regular or altered metabolism [10–12, 16–18]. Therefore, for consumed metabolites, a decrease in the detected amount corresponds to an increase in the consumption, and vice-versa. Regarding the levels of excreted substances, a simple direct relationship can be held in the analysis. Table 1 presents a list of metabolites originally present in the culture media labeled as "§" that can be consumed and those excreted by cells with no label.

Under the basal condition and addressing the case where culture media are available in two specific periods of time, 48 h and 96 h, we found three {mDB}, as summarized in Fig. 5B. Valine and tyrosine, both aminoacids consumed by cells, presented low concentrations for those media collected with 48 h of incubation, on average ~9% (Table 2), when compared with collected with 96 h, meaning that cells with more time in culture are down-regulating the rate of consume of these specific amino acids. An analogous tendency of low levels for the first 48 h of cell incubation was detected for 3-methylhistidine, indicating that CMs elevate the excretion of this metabolite by ~15% (Table 2) in the second period of incubation. Valine and tyrosine could be consumed by CMs to be used in converged biosynthesis [25] to produce succinil-CoA from Val and acetyl-CoA or fumarate, from Tyr. On the other hand, we could argue about the origin of 3-MHis in the cellular environment as intermediates produced in histidine metabolism [29], which seems to be upregulated by basal CMs over time. Dimethylamine, also a metabolite excreted by cells, was decreased by almost 100% in the second period of incubation, suggesting intense activity of the metabolic pathway in which this organic secondary amine is intermediary in the first 48 h of culture, which seems to cease in the last incubation period. Interestingly, this tendency repeats in both incubators and both conditions, basal and HfR; therefore, it could be considered as a robust metabolic event occurring with CMs in general.

For the dynamic metabolites evaluated in the HfR event, {mDHR}, we found seven classifier molecules, as summarized in Fig. 5C. The quantitative analysis for these metabolites consumed by CMs were plotted in Fig. 5F that revealed an increase in the rate of consumption of "§"-metabolites on average $23.8 \pm 5.3\%$ for the first 48 h comparatively to last incubation period demonstrating an intense cellular activity in this group of cells taking place in the first stage of incubation. As referred before, Leu, Ile, Met, and Thr are amino acids involved in processes of converged cellular biosynthesis of a few complex molecules via degradation of their respective carbonic chains [25] such as those processed in glycolysis or TCA using exogenous components obtained from culture media. For instance, pyruvate can be synthesized from Thr, acetyl-CoA from Leu, Ile, and Thr, while succinyl-CoA from Ile, Met, and Thr. We now observe a reasonable convergence between the results obtained for samples of cellular extracts and culture media related to the set of metabolites ascribed to the effect of HfR, which are quite equivalent and even complement each other, as in the case of methionine and threonine detected in the culture media involved in the converged biosynthesis of succinyl and acetyl coenzymes. It is important to mention that for the case of cell samples, the information generated by the endometabolome came from the result of the accumulated metabolism after 96 h of incubation, while for culture media we have the information obtained from the exometabolome at 96 h, corresponding to that obtained for cells and also for 48 h in a dynamic analysis approach. This metabolic overview demonstrates that cardiomyocytes dynamically regulate part of their energetic metabolism, making use of aminoacid degradation processes that could be supplied from proteins, more intensely in the first 48 h. We attribute to this cellular response the extreme challenge induced by HfR experiment that produces elevated rates of death for this group in comparison with basal. To conclude the analysis of this case we will address the quantitative results summarized through the {mDHR}, which were excreted by CMs, as shown in Fig. 5G. As can be seen in this figure and comparison [HRh48 *vs*. HRh96] of Table 2, their respective levels decrease for the first 48 h compared to 96 h, indicating they were being more excreted in the last cycle of incubation. Analyzing the metabolic pathways from which they are biochemical intermediates, we have further evidence of how stressed

CMs can auto-regulate different parts of their metabolism in response to the HfR event. For instance, acetone is a ketone body derived from spontaneous decarboxylation of acetoacetate. This last can be produced in situations where acetyl-CoA is available in excess inside the mitochondrial matrix and signalizes ketogenic stress [10]. Thus, this finding supports the premise that CMs undergoing HfR can upregulate the synthesis of acetyl-CoA besides showing that cells are passing through ketogenic stress in both periods of cell incubation, but more intensely in the second one. This finding can be supported in the premise that a reduced population of CMs, that suffered the deadly consequences of HfR, are simply consuming less acetyl-CoA than the basal group. Besides, they are passing through ketogenic stress in both periods of cell incubation, but more intensely in the second one.

Addressing the case of time-persistent HfR metabolites, that is, those that repeat themselves as classifiers of HfR events over the past 48 h (Fig. 6A) and 96 h (Fig. 6B) of CMs metabolism evaluated through the media samples, these are summarized in Fig. 5D, E, discriminating which they are, while Fig. 5F, G show their quantitative tendencies to change the levels. For media collected after 48 h of CMs incubation, there is a possibility of converged biosynthesis occurring [25] as schematized in Fig. 6A: on anaerobiosis, pyruvate from threonine and alanine; on aerobiosis, acetyl-CoA from leucine, isoleucine, threonine, and tyrosine; succinyl-CoA from isoleucine, methionine, and threonine; and fumarate from tyrosine. In all these biochemical conversions, it was observed that stressed cells increased the consumption of these amino acids compared to basal ones (Fig. 6A), so it is reasonable to argue that more of these complex molecules are being produced by treated cells, at least for the first 48 h of CMs incubation. This situation tends to regularize for the last 48 h of CMs incubation (Fig. 6B) once the number of {mPHR} metabolites is dramatically reduced, suggesting that the metabolism of both groups of CMs, those undergoing HfR and the basal ones, seems to converge, at least in terms of energy production mechanisms.

Despite our analyses addressing, in general, the production of energy by cells from processes concerning the degradation of carbonic chains of amino acids, whether they come from proteins (endogenous) or culture medium (exogenous), cells can also produce their energy from the degradation of carbohydrate carbonic chains, such as glucose, a monosaccharide with an aldehyde function. In fact, the degradation of carbohydrates in the cellular respiratory chain is usually the first alternative for energy production by cells under basal conditions. However, when energy demand increases dramatically in a short time, carbohydrate reserves are rapidly depleted, pushing cells to choose other alternatives such as the degradation of amino acids or proteins, this being the reason why we are exploring this last metabolic pathway in detail. Although the results found for cell samples do not provide evidence of the consumption of the glucose molecule present in the media samples, it can produce two important metabolites that are products of its energy metabolism: pyruvate, resulting from anaerobic glycolysis, and lactate, resulting from lactic fermentation. Our previous results suggested that stressed CMs do not produce lactate molecules once the associated resonance signals have lower area values (< 0.001). This tendency indicates that in this case, cells choose down-regulated lactic metabolism when compared to basal metabolism, which, in a certain way, agrees with the results found in the culture media samples that showed accentuated consumption of amino acids with protein origins.

The results found for culture media samples regarding glucose molecules can help to support our premise summarized in the last paragraph. For instance, we did not detect that it was confirmed as a classifier between the dynamic comparisons (48 h vs. 96 h) for basal and stressed groups as can be seen in the Fig. 5B, C. This result suggests that both groups may consume glucose at their own rates that seem to remain constant throughout the period of time that the cells were kept in culture, that is, at 96 h. Finally, with respect to the persistent comparisons, stressed *versus* basal at 48 h and 96 h, summarized in Fig. 5D, E, glucose is a classifier in the analysis, always showing an excess for CMs undergoing HfR (Fig. 5F) which can being interpreted as a lesser preconditioned cells population, then less glucose consumed. Additionally, we could extend this observation to argue that stressed CMs use less energy resources than basal CMs, which agrees with the premise that the effect of HfR technique activates mechanisms of degradation of carbonic chains of aminoacids of protein origin driving the synthesis of more complex. Consequently, there are more energetic molecules as the coenzymes used in TCA and this is a phenomenon that can persist in the two periods of time investigated. In fact, this metabolic scenario also seems to occur in the basal case, but with quite different metabolic consumption rates than stressed CMs.

Pyroglutamate is an intermediate in glutathione biosynthesis that is excreted by cells to the media and plays an essential role in reducing inactive oxidized proteins by removing disulfide bridges. As shown in Fig. 5G, the rate of pyroglutamate excretion by CMs undergoing HfR remained increased by ~23% when compared to basal at both periods of time evaluated (persistent changing), particularly in the last 48 h cycle, indicating that glutathione biosynthesis may be upregulated by stressed cells (Fig. 6A, B). If more pyroglutamate is excreted by cells into the culture medium compared to the control then those treated probably drive their metabolism to elevate the production of antioxidant agents such as glutathione as response of ROS induction [10–12, 16–18].

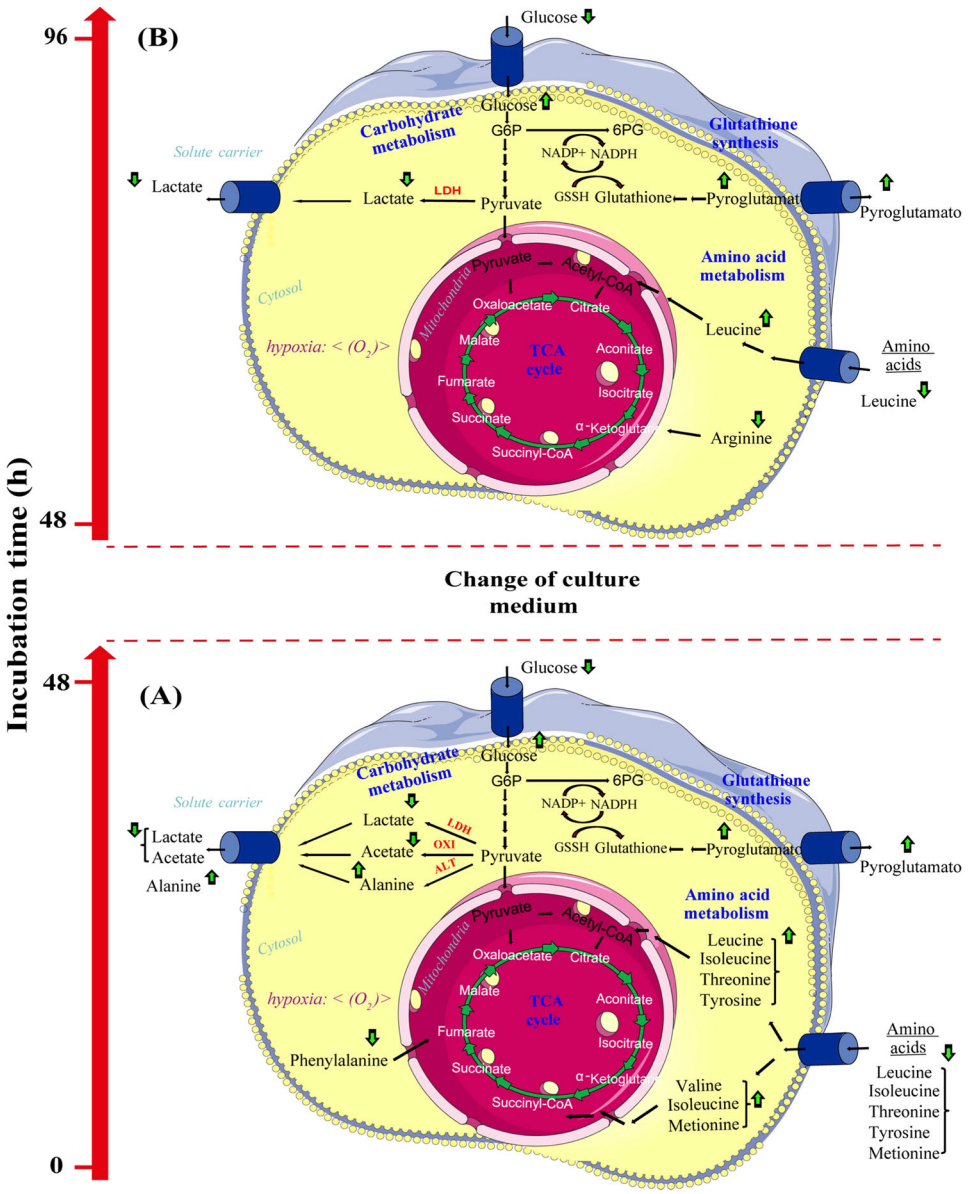

Fig. 6 Summary of identified metabolic pathways that change with HfR treatment at two different incubation times for different culture media (**A**) 0–48 h and (**B**) 48–96 h, showing tendencies of increase/decrease in metabolite levels, as shown in Fig. 5F, G. G6P glucose 6-phosphate, 6PG 6-phosphogluconate, GSSH oxidized glutathione, LDH lactate dehydrogenase, OXI oxidation, ALT for Alanine aminotransferase, TCA tricarboxylic acid cycle. Figure adapted from "Servier Medical ART," a repository of free medical images provided by Les Laboratoires Servier (http://smart.servier.com) and licensed under a Creative Commons Attribution 3.0 Unported License

Figure 5G also shows succinate (e363), not present in the original elements of culture media, with a reduced excretion rate by stressed CMs when compared to basal ones for culture media collected at 48 h. This is precisely the period of time in which supposedly cells auto-regulate their metabolism in a very intense way until a metabolic pattern close to basal cells is achieved in the subsequent 48 h period. Succinate is a molecule that plays an important role in TCA metabolism [30], acting as a biochemical bridge between the conversion of succinyl-CoA into fumarate, providing direct evidence of a detected molecule through resonance data. This tendency seems to indicate that stressed CMs probably make use of this molecule to produce their energetic requirements more intensely than basal cells in the first incubation period, once it is less excreted. Finally, regarding acetate, AcOH, our results demonstrated that this classifier metabolite was decreased for CMs undergoing HfR when compared to basal for culture media collected at 48 h (Fig. 5G). This metabolite is involved in pyruvate oxidation in the carbohydrate metabolism that could be used by cells to produce acetyl-CoA [31]. However, when pyruvate diverges to the TCA it are oxidized to AcOH, thus indicating that stressed cells drive most of their acetyl-CoA production from carbohydrate resources to be used as important resource for TCA in order to balance their energetic metabolism when the effects of induced hypoxic stress are quite intense, i.e., in the first 48 h of incubation.

As described early by Savla et al. [32], chronic hypoxia has mixed effects on cardiovascular health, whether it is beneficial or detrimental depends on the specific pathophysiologic context

and patient risk factors. However, the hypoxic situation pushes the heart to evolve a delicate adaptive program to maintain metabolic efficiency, in which glucose becomes preferentially used over fatty acid for ATP production [33]. For instance, Ross-Ascuitto et al. [34] observed that chronically hypoxic rabbits exposed to 10% O_2 for up to 5 weeks, their hearts exhibited enhanced ventricular function and increased capacity for glucose oxidation compared to normoxic counterparts. On the other hand, Ferrannini et al. [35] show that the oxidation of ketones bodies is comparable to glucose and pyruvate in terms of oxygen efficiency, which makes it an equally efficient fuel under metabolically stressed conditions. Our main findings also indicate changes in the energetic resources by the stressed cells in order to compensate for the momentaneous lack of oxygen. For instance, despite the carbohydrate metabolism detected in the endometabolome indicates that it was similarly accessed by stressed and unstressed CMs, when the comparisons were performed using the exometabolome, the first group of CMs tends to consume less glucose for the same incubation period of 96 h. Additionality, the two obtained exometabolomes profiles, at 48 h and 96 h, depicted a set of consumed aminoacids by stressed cells tending to increase when compared to unstressed and this pattern can be directly related with the increases in biosynthesis of acetyl-CoA, a primary energetic substrate for TCA, occurring for those CMs suffering through HfR. Changing in the rates of acetone production, a ketone body, detected only in the exometabolomes of stressed CMs at 48 h and 96 h, also proves that cells are making use of this type of energetic substrate as we described before, besides to signalize the presence of ketogenic stress. Thus, all these detected metabolic changes are indicators of transformations induced by hypoxia in a cellular life-scale where, in order to keep the metabolic efficiency, stressed cells are dynamically exchanging their energetic resources primarily to conserve TCA running even despite the low oxygen concentrations. Thus, the inference about biosynthesis up-regulation of coenzymes, such as acetyl-CoA, proposed here from the obtained set of aminoacids, besides that generated by pyruvate oxidation in carbohydrate metabolism evaluated from glucose levels, seems to be quite robust for CMs undergoing HfR.

Conclusion

In this study we designed, built, and tested a special device named hypoxia incubator capable of inducing cellular stress by HfR in non-proliferative cardiomyocytes used to evaluate how catabolic/anabolic metabolisms, such as those involving carbohydrates and proteins, are time evolving in response to stress induced by repeated cycles of hypoxia. To achieve this goal, metabolomics based on proton magnetic resonance spectroscopy was applied to samples obtained from cellular extracts and culture media. To account for issues concerning incubator efficiency and basal metabolism of cells that could mask the real effects of hypoxia events, we proposed a reasonable strategy for isolating metabolic effects through selective comparisons among the samples that resulted in five groups of landmark metabolites enabling us to achieve a more realistic overview of metabolic changes, both qualitatively and quantitatively.

Our analysis indicated that stressed cells promoted intense metabolic changes in the first 48 h of culture when the highest variations in metabolites levels involved in the biosynthesis of complex molecules, such as pyruvate, acetyl-CoA, succinyl-CoA, and fumarate, through the aminoacid up-regulating metabolism to produce a pool of energetic substrates directed to TCA was observed as a response to oxygen deficiency. This situation tends to be regularized for the last 48 h HfR cycle with a metabolic pattern presenting similarities to basal cells. Additionally, it was observed that carbohydrate metabolism seems to be accessed by both groups of cells for the past 96 h of incubation without showing significant intra-group differences; however, when the comparisons were performed between stressed and unstressed samples, inter-group, the first tending to consume less glucose during the same period of incubation. Our data also indicate that most of the pyruvate generated in cellular environments by stressed groups originates from the breakdown of carbonic chains of aminoacids molecules in detriment of those produced from carbohydrates. In addition, the destination for pyruvate is the conversion to acetyl-CoA to be used, for instance, in TCA; besides a low level of excreted acetate due to the pyruvate oxidation was detected by stressed cells (down-regulated route). This scenario supposes that both groups of cardiomyocytes make use of all glucose available in the cellular environment that is directed to carbohydrate metabolism to be used as a primary source of energy production, each with its own way of consumption. The primary sources of aminoacids present in the cellular environments could be of endogenous origin, such as active protein degradation by cells, as demonstrated by our analysis of cellular extract samples, or exogenous, such as the consumption of components of culture media, as demonstrated by analysis of culture media samples. In addition, the rich pyroglutamate environment suggests balancing the excess of ROS. The challenge that shows up now is to calibrate the times of hypoxia treatment in order to induce minimal cellular deaths, lower than 5%, and verify whether the general metabolic status found in this work still holds and, for this, further studies are imperative.

Data Availability

Experimental data, statistical analysis results, protocols used for cell manipulation, and hypoxia incubator electric

schemes that supported this study can be found within the paper, in the supplementary materials or can be provided from the corresponding author on reasonable request.

Supplementary Information The online version contains supplementary material available at https://doi.org/10.1007/s12013-024-01249-1.

Acknowledgements The authors would like to acknowledge the Sao Paulo Research Foundation - FAPESP (grants 2011/19678-1; 2013/17368-0; 2014/22102-2; 2014/21646-9; 2018/20910-5), and Medical Sciences Graduate Program-CAPES/PROEX for financial support; Instituto de Pesquisas Tecnologicas (IPT) for providing NMR spectrometer and facilities; Laboratory of Genetics and Molecular Cardiology, Heart Institute (InCor), University of Sao Paulo School of Medicine for providing cells and scientific assistance; and National Institute of Science and Technology Complex Fluids (INCT-FCX) for daily financial aid.

Author Contributions L.D.M.C. and A.C.B. contributed to design, coding, calibrations, and the first trials with cells in the HI device. A.C.B. contributed performing all the resonance experiments, biological interpretations, and drafted the entire manuscript. L.D.M.C. contributed to the cell experiments, sample preparation, viability assays, resonance data processing, and statistical analysis. Y.B.B. and C.V.V. made suggestions and corrections to the manuscript. L.F.G. contributed to the revision of biological interpretations of the results and its respective discussions. C.V.V. drew Fig. 6. All authors contributed to the revision of the manuscript and agreed to be fully accountable for ensuring the integrity and accuracy of the work and reading and approving the final manuscript.

Compliance with Ethical Standards

Conflict of interest The authors declare no competing interests.

Ethical approval Approval was obtained from the institutional review board of the University of Sao Paulo, School of Medicine, Brazil (#340/12).

References

1. Virani, S. S., Alonso, A., Benjamin, E. J., Bittencourt, M. S., Callaway, C. W. & & Carson, A. P. American Heart Association Council on Epidemiology and Prevention Statistics Committee and Stroke Statistics Subcommittee. (2020). Heart disease and stroke statistics-2020 update: A report from the American Heart Association.*Circulation*, *141*(9), e139–e596. https://doi.org/10.1161/CIR.0000000000000757.
2. Flora, G. D., & Nayak, M. K. (2019). A brief review of cardiovascular diseases, associated risk factors and current treatment regimes. *Current Pharmaceutical Design*, *25*(38), 4063–4084. https://doi.org/10.2174/1381612825666190925163827.
3. Fryar, C. D., Chen, T.-C., & Li, X. (2012). Prevalence of uncontrolled risk factors for cardiovascular disease: United States, 1999-2010. *NCHS Data Brief*, *103*, 1–8
4. Oprea, A. D., Russell, R. R., Russell, K. S., & Abu-Khalaf, M. (2017). Chemotherapy agents with known cardiovascular side effects and their anesthetic implications. *Journal of Cardiothoracic and Vascular Anesthesia*, *31*(6), 2206–2226. https://doi.org/10.1053/j.jvca.2015.06.020.
5. Bilo, G., Gatterer, H., Torlasco, C., Villafuerte, F. C., & Parati, G. (2022). Editorial: Hypoxia in cardiovascular disease. *Frontiers in Cardiovascular Medicine*, *9*, 990013. https://doi.org/10.3389/fcvm.2022.990013.
6. Parati, G., Agostoni, P., Basnyat, B., Bilo, G., Brugger, H., Coca, A., & Torlasco, C. (2018). Clinical recommendations for high altitude exposure of individuals with pre-existing cardiovascular conditions: A joint statement by the European Society of Cardiology, the Council on Hypertension of the European Society of Cardiology, the European Society of Hypertension, the International Society of Mountain Medicine, the Italian Society of Hypertension and the Italian Society of Mountain Medicine. *European Heart Journal*, *39*(17), 1546–1554. https://doi.org/10.1093/eurheartj/ehx720.
7. Parati, G., Bilo, G., Faini, A., Bilo, B., Revera, M., Giuliano, A., & Mancia, G. (2014). Changes in 24 h ambulatory blood pressure and effects of angiotensin II receptor blockade during acute and prolonged high-altitude exposure: A randomized clinical trial. *European Heart Journal*, *35*(44), 3113–3122. https://doi.org/10.1093/eurheartj/ehu275.
8. Lucero García Rojas, E. Y., Villanueva, C., & Bond, R. A. (2021). Hypoxia inducible factors as central players in the pathogenesis and pathophysiology of cardiovascular diseases. *Frontiers in Cardiovascular Medicine*, *8*, 709509. https://doi.org/10.3389/fcvm.2021.709509.
9. Chen, X.-Y., Wang, J.-Q., Cheng, S.-J., Wang, Y., Deng, M.-Y., Yu, T., & Zhou, W.-J. (2021). Diazoxide Post-conditioning Activates the HIF-1/HRE Pathway to Induce Myocardial Protection in Hypoxic/Reoxygenated Cardiomyocytes. *Frontiers in Cardiovascular Medicine*, *8*, 711465. https://doi.org/10.3389/fcvm.2021.711465.
10. Bloise, A. C., Dos Santos, J. A., de Brito, I. V., Bassaneze, V., Gomes, L. F., & Alencar, A. M. (2020). Discriminating aspects of global metabolism of neonatal cardiomyocytes from wild type and KO-CSRP3 rats using proton magnetic resonance spectroscopy of culture media samples. *In Vitro Cellular & Developmental Biology. Animal*, *56*(8), 604–613. https://doi.org/10.1007/s11626-020-00497-8.
11. Palomares, C. V. V., Barreto, Y. B., Bexiga, N. M., Toma, S. H., Julival dos Santos, J., Araki, K., … Bloise, A. C. (2023). Metabolic profiling of murine macrophages exposed to silver nanoparticles at dose and time dependencies. *Particle & Particle Systems Characterization*, 2200191. https://doi.org/10.1002/ppsc.202200191
12. Vivas, C. V., dos Santos, J. A., Barreto, Y. B., Toma, S. H., dos Santos, J. J., Stephano, M. A., … Bloise, A. C. (2023). Biochemical response of human endothelial and fibroblast cells to silver nanoparticles. *BioNanoScience*. https://doi.org/10.1007/s12668-023-01091-4
13. Campos, L. C. G., Ribeiro-Silva, J. C., Menegon, A. S., Barauna, V. G., Miyakawa, A. A., & Krieger, J. E. (2018). Cyclic stretch-induced Crp3 sensitizes vascular smooth muscle cells to apoptosis during vein arterialization remodeling. *Clinical Science*. https://doi.org/10.1042/CS20171601
14. Jensen, L., Neri, E., Bassaneze, V., De Almeida Oliveira, N. C., Dariolli, R., Turaça, L. T., & Krieger, J. E. (2018). Integrated molecular, biochemical, and physiological assessment unravels key extraction method mediated influences on rat neonatal cardiomyocytes. *Journal of Cellular Physiology*, *233*(7), 5420–5430. https://doi.org/10.1002/jcp.26380.
15. Freshney, R. I. (2010). *Culture of animal cells: A manual of basic technique and specialized applications*. Hoboken, NJ, USA: John Wiley & Sons, Inc. https://doi.org/10.1002/9780470649367.
16. Martins-Bach, A. B., Bloise, A. C., Vainzof, M. & & Rahnamaye Rabbani, S. (2012). Metabolic profile of dystrophic mdx mouse muscles analyzed with in vitro magnetic resonance spectroscopy (MRS).*Magnetic Resonance Imaging*, *30*(8), 1167–1176. https://doi.org/10.1016/j.mri.2012.04.003.

17. Bacchi, P. S., Bloise, A. C., Bustos, S. O., Zimmermann, L., Chammas, R., & Rabbani, S. R. (2014). Metabolism under hypoxia in Tm1 murine melanoma cells is affected by the presence of galectin-3, a metabolomics approach. *SpringerPlus*, *3*, 470. https://doi.org/10.1186/2193-1801-3-470.
18. Lindon, J. C., Holmes, E., & Nicholson, J. K. (2006). Metabonomics techniques and applications to pharmaceutical research & development. *Pharmaceutical Research*, *23*(6), 1075–1088. https://doi.org/10.1007/s11095-006-0025-z.
19. Madsen, R., Lundstedt, T., & Trygg, J. (2010). Chemometrics in metabolomics–a review in human disease diagnosis. *Analytica Chimica Acta*, *659*(1–2), 23–33. https://doi.org/10.1016/j.aca.2009.11.042.
20. Worley, B., & Powers, R. (2013). Multivariate analysis in metabolomics. *Current Metabolomics*, *1*(1), 92–107. https://doi.org/10.2174/2213235X11301010092.
21. Wu, Z, Li, D, Meng, J. & Wang, H. (2010). Introduction to SIMCA-P and its application. In: V. Esposito Vinzi, W. W. Chin, J. Henseler & H. Wang, (Eds.) *Handbook of partial least squares* (pp. 757–774). Berlin, Heidelberg: Springer Berlin Heidelberg. https://doi.org/10.1007/978-3-540-32827-8_33
22. Xia, J., & Wishart, D. S. (2016). Using metaboanalyst 3.0 for comprehensive metabolomics data analysis. *Current Protocols in Bioinformatics*, *55*, 14.10.1–14.10.91. https://doi.org/10.1002/cpbi.11.
23. Bilal Zorić, A. (2021). Applied statistics: basic principles and application. *International Journal of Industrial Electronics and Drives*, *7*(3), 27–33. https://doi.org/10.18775/ijied.1849-7551-7020.2015.73.2003.
24. Triba, M. N., Starzec, A., Bouchemal, N., Guenin, E., Perret, G. Y., & Le Moyec, L. (2010). Metabolomic profiling with NMR discriminates between biphosphonate and doxorubicin effects on B16 melanoma cells. *NMR in Biomedicine*, *23*(9), 1009–1016. https://doi.org/10.1002/nbm.1516.
25. Tansey, J. T., Baird, T., Cox, M. M., Fox, K. M., Knight, J., Sears, D., & Bell, E. (2013). Foundational concepts and underlying theories for majors in "biochemistry and molecular biology". *Biochemistry and molecular biology education: a bimonthly publication of the International Union of Biochemistry and Molecular Biology*, *41*(5), 289–296. https://doi.org/10.1002/bmb.20727.
26. Zhang, J., Wang, Y. T., Miller, J. H., Day, M. M., Munger, J. C., & Brookes, P. S. (2018). Accumulation of succinate in cardiac ischemia primarily occurs via canonical krebs cycle activity. *Cell Reports*, *23*(9), 2617–2628. https://doi.org/10.1016/j.celrep.2018.04.104.
27. Prochownik, E. V., & Wang, H. (2021). The metabolic fates of pyruvate in normal and neoplastic cells. *Cells*, 10(4). https://doi.org/10.3390/cells10040762
28. Watt, I. N., Montgomery, M. G., Runswick, M. J., Leslie, A. G. W., & Walker, J. E. (2010). Bioenergetic cost of making an adenosine triphosphate molecule in animal mitochondria. *Proceedings of the National Academy of Sciences of the United States of America*, *107*(39), 16823–16827. https://doi.org/10.1073/pnas.1011099107
29. Aliu, E., Kanungo, S., & Arnold, G. L. (2018). Amino acid disorders. *Annals of translational medicine*, *6*(24), 471 https://doi.org/10.21037/atm.2018.12.12.
30. Prasun, P. (2019). Disorders of pyruvate metabolism and tricarboxylic acid cycle. In *Mitochondrial Medicine* (pp. 83–95). Elsevier. https://doi.org/10.1016/B978-0-12-817006-9.00015-0
31. Kanehisa, M., Furumichi, M., Sato, Y., Ishiguro-Watanabe, M., & Tanabe, M. (2021). KEGG: integrating viruses and cellular organisms. *Nucleic Acids Research*, *49*(D1), D545–D551. https://doi.org/10.1093/nar/gkaa970.
32. Savla, J. J., Levine, B. D., & Sadek, H. A. (2018). The effect of hypoxia on cardiovascular disease: friend or foe. *High Altitude Medicine & Biology*, *19*(2), 124–130. https://doi.org/10.1089/ham.2018.0044.
33. Su, Z., Liu, Y., & Zhang, H. (2021). Adaptive cardiac metabolism under chronic hypoxia: mechanism and clinical implications. *Frontiers in cell and developmental biology*, *9*, 625524 https://doi.org/10.3389/fcell.2021.625524.
34. Ross-Ascuitto, N. T., Joyce, J. J., Hasan, A. Z. M. A., & Ascuitto, R. J. (2004). Performance of the chronically hypoxic young rabbit heart. *Pediatric Cardiology*, *25*(4), 397–405. https://doi.org/10.1007/s00246-003-0429-z.
35. Ferrannini, E., Mark, M., & Mayoux, E. (2016). CV Protection in the EMPA-REG OUTCOME Trial: A "Thrifty Substrate" Hypothesis. *Diabetes Care*, *39*(7), 1108–1114. https://doi.org/10.2337/dc16-0330.